Estimating the Inter-fiber Bonding Capacities of High-yield Pulp (HYP) Fibers by Analyzing the Fiber Surface Lignin and Surface Charge

Hailong Li,[a,b] Hongjie Zhang,[a,c,d]* Sarah Legere,[b] Yonghao Ni,[a,b] Xuejun Qian,[c] Hongshun Cheng,[c] Fengshan Zhang,[d] and Xiaoliang Li [d]

Four fiber fractions from poplar alkaline peroxide mechanical pulping, performed with refiner-chemical preconditioning (P-RC APMP), were used to estimate inter-fiber bonding capacity. The relationship between fiber characteristics and inter-fiber bonding capacities was investigated. The surface lignin content of the long fiber fraction was slightly lower than that of the short fiber fraction. Atomic force microscopy (AFM) images showed that the fiber surfaces were heterogeneous (*i.e.*, different cell wall layers were exposed along the fiber surface). The fiber fractions that had lower surface lignin content had higher bonding capacities. Furthermore, modified PFI beating was used to peel the surface of the fibers. After the peeling treatment, the fiber surface charge increased remarkably, while the surface lignin concentration decreased considerably. The lignin and charge on the fiber surface are the two key factors for estimating the inter-fiber bonding capacities.

*Contact information: a: Tianjin Key Lab of Pulp & Paper, Tianjin University of Science & Technology, Tianjin 300457, China; b: Limerick Pulp and Paper Centre, University of New Brunswick, Fredericton, NB E3B 5A3, Canada; c: Hebei Huatai Paper Industry Co. Ltd., Huatai Group, Zhaoxian 051530, China; d: Shandong Huatai Paper Industry Co. Ltd., Huatai Group, Dongying 257335, China; * Corresponding author: hongjiezhang@tust.edu.cn*

INTRODUCTION

The development of biomass-derived materials has been receiving increased attention due to the need for sustainable green chemistry processes and materials (Ragauskas *et al.* 2006). As the main biomass-derived material in use currently, lignocellulosic fibers derived from plants are particularly attractive for incorporation into advanced materials due to their ubiquitous renewable production, facile isolation, and strength properties (Lei *et al.* 2012; Ranganathan *et al.* 2016). Lignocellulosic fibers have been extensively investigated for potentially unique applications in paper and paperboard (Shen and Fatehi 2013), composites (Faruk *et al.* 2014), and as scaffolds for tissue engineering (Qazi *et al.* 2015).

As a type of lignocellulosic fiber, high yield pulps (HYPs) have become important components in a variety of paper grades (Li *et al.* 2014). Compared with bleached chemical pulps, HYPs have a high bulk, opacity, and light scattering coefficient, but their main drawback is their weak inter-fiber bonding strength, which limits the application of HYPs in value-added products (Li *et al.* 2014, 2015). In the past decade, a kind of HYPs, P-RC APMP has achieved widespread application in many paper and paper-based products in worldwide, especially in China (Li *et al.* 2014; Zhao *et al.* 2016).

The factors that affect the bonding ability of lignocellulosic fibers are fiber morphology (*e.g.*, the average fiber length and width, fiber coarseness, fines content, kink index, *etc.*), chemical content (*i.e.*, the ratio of cellulose, hemicellulose, lignin, and extractives), and the fiber charge (Zhao *et al.* 2016). Fiber morphology is the basic characteristic of lignocellulosic fibers. It influences the strength properties and the papermaking properties of fibers from different materials and manufacturing processes (Li *et al.* 2015). The fiber length, fiber coarseness, and fines content are the key factors affecting fiber strength properties. The flexibility, deformability, and the strength properties of the fibers are determined by their chemical makeup (Li *et al.* 2016). HYPs have more residual lignin than bleached chemical pulps, resulting in a higher yield. Unlike cellulose and hemicelluloses, lignin is a hydrophobic material. The lignin of HYP fibers, especially the surface lignin covering the cellulose and hemicelluloses, which have free hydroxyl groups, hinders the formation of hydrogen bonds between fibers (Shao and Li 2006).

In the papermaking process, there are fiber-fiber and fiber-additive interactions on the fiber surfaces. In the final paper sheet, fiber-fiber bonding occurs on the surface of the fibers (Hubbe 2007). Therefore, the surface chemistry and morphology of the fibers largely determine the inter-fiber bonding and hence the physical strength of the fiber network (Shen *et al.* 2014). For HYP fibers, the fiber surface deformations are the result of fiber separation in the refining process. If fibers separate in the middle lamella region, the resulting fibers have additional middle lamella material on their surface, whereas if fiber separation occurs in the secondary wall, more cellulose is exposed on the fiber surface. Therefore, it is possible to design different processes for producing a desired fiber surface.

The chemical composition on the fiber surface plays an important role in inter-fiber bonding. Shao and Li determined the effect of the surface lignin on inter-fiber bonding, and found that fiber surface lignin covered the cellulose and hemicelluloses, and hindered the formation of hydrogen bonds (Shao and Li 2006). The determination and control of the surface lignin content and its distribution are important for the optimization of the pulping and papermaking process.

In this study, a poplar P-RC APMP pulp was used as a raw material to estimate the inter-fiber bonding capacities of HYP fibers. The key parameters of the inter-fiber bonding capacities were determined, such as the bonding strength index (B), the specific bonding strength per unit bonded area (b), and the relative bonded area (RBA). The morphology, fiber charge, and lignin content on fiber surfaces were investigated to assess how these factors affect the inter-fiber bonding capacity. Furthermore, a modified PFI beating treatment was applied to induce peeling on the fiber surface, and the influence of the surface lignin on the inter-fiber bonding capacities of the HYP fibers was investigated.

EXPERIMENTAL

Materials

A poplar P-RC APMP pulp, collected from a pulp mill in Shandong province, China, was classified with a Bauer-McNett fiber classifier (8901-05, TMI GROUP, New Castle, DE, USA) into different fiber fractions according to TAPPI method T233 cm-95 (1995). The fiber fractions included R30, P30/R50, P50/R100, and P100/R200. The R30 and P30/R50 were the long-fiber fractions, the P50/R100 was the middle-fiber fraction, and the short-fiber fraction was the P100/R200. Before measuring the lignin content, the

different fiber fractions were extracted with organic solvent (a benzene and ethanol mixed with a volume ratio of 2:1). This procedure removed the extractives according to standard method GB/T10741 (1989). The fibers were then cleaned with deionized water to remove residual organic solvent. Finally, the fibers were air-dried and stored.

Methods

The characterization of fiber morphology

The fiber morphology characteristics were measured using a Fiber Tester (L&W921, Kista, Sweden), including average of fiber length and width, and coarseness. Each time, more than 5,000 fibers were used for the fiber testing and the statistical average values were obtained.

The total lignin content and fiber charge of different fiber fractions

The total lignin content of four fiber fractions was computed by adding the corresponding Klason lignin and acid-soluble lignin. The measurement of Klason lignin content was computed following the GB/T747 (1989) standard, while the acid-soluble lignin content was measured with an ultraviolet spectrophotometer (UV-2550, Shimadzu, Tokyo, Japan) according to GB/T10337 (1989).

The characterization of fiber charge was obtained following the method of Zhao *et al.* (2016), which is depending on the poly-DADMAC accessibility to cellulose fibers. The determination of the fiber charge has four steps: 1) protonated form of the fibers (or removing the metal ions in the fibers) was prepared by soaking the fibers with overdosed 0.01 M HCL, then the fibers were filtered by using Büchner funnel and washed several times with deionized water until the conductivity of filtrate was below 5 μS/cm; 2) sodium form of the fibers was prepared by soaking the fibers in 10^{-3} M $NaHCO_3$ solution, then the fibers were filtered and washed as same as step 1; 3) the fibers in its sodium form were dispersed in two kinds of excess 10^{-3} N poly-DADMAC solutions respectively (the poly-DADMAC with M_w of 11 kDa and charge density of 6.05 meq/g was used for the determination of total charge, while the poly-DADMAC with M_w of 260 kDa and charge density of 6.10 meq/g was used for the determination of fiber surface charge); 4) the fibers were filtered and the filtrate was titrated in a MÜTEK particle charge detector (PCD-03, Germany) and 10^{-3} N PVSK solution was used for the polyelectrolyte titration. The blank values were determined by titrating the same volume of 10^{-3} N poly-DADMAC solutions; 5) the total and surface charge of the fibers was calculated following the Eq. 1 (Zhao *et al.* 2016),

$$q = \frac{(V_b - V_p)c}{w} \tag{1}$$

where *q* is the detected charge of the fibers (mmol/kg), V_b is the blank value (ml), V_p is the volume of the PVSK used for titrating the filtrate (ml), *c* is the concentration of the PVSK (mol/l), and *w* is the weight of the fibers used for the charge determination (g).

Surface analysis by XPS and AFM technique

X-ray photoelectron spectroscopy (XPS) measurements were performed with an X-ray photoelectron spectrometer system (K-α, Thermo Fisher, Waltham, USA). The area of the X-ray measurement was 500×500 μm, and the samples were mounted on a sample holder and outgassed overnight under a pressure of 1×10^{-9} Torr. Each sample was measured at three different spots, and the results were averaged. The XPS spectra were obtained with

a photoelectron take-off angle of 90° relative to the sample surface. To avoid X-ray damage on the fiber surface, the measurement time was limited to 30 min.

The samples for atomic force microscope (AFM) measurement were prepared by dropping a well-dispersed fiber suspension onto the surface of mica and then air-drying the sample at ambient temperature. AFM imaging was performed using a multi-purpose and high-resolution scanning probe microscope (JSPM-5200, JEOL Ltd., Tokyo, Japan). Silicon AFM probes from Budget Sensors (Tap300AI-G, Sofia, Bulgaria) had a resonant frequency of 300 kHz and force constant of 40 N/m. Prior to AFM imaging, the micas with dried fibers attached were placed on sample stubs covered by double-sided adhesive tape. All images were scanned in tapping mode in air. Images of at least five different fibers were scanned for each sample.

Removal of the surface lignin by PFI beating

The P30/R50 fiber fraction was used for the removal of the surface lignin by PFI beating. The modified PFI refining focuses on peeling the fiber surface. The consistency of pulp fibers for PFI beating was 20%, while one of the balance weights in PFI mill was removed and the gap clearances between the bedplate and roll in PFI mill was set at 2 mm. The different revolutions of the PFI beating were set to produce samples with different surface lignin content.

Measurement of the bonding capacities of HYP fiber

The fibers for the measurement of the bonding capacities were made into handsheets according to TAPPI T205 sp-95 (1995). A laboratory sheet former (RK-3A, PTI, Vorchdorf, Austria) and an automatic sheet press (No. 2571-I, KRK, Tokyo, Japan) were used in this step. The light-scattering coefficient, tensile index, and zero-span tensile index of handsheets were tested, respectively, using an Elrepho spectrophotometer (L&W SE070, Kista, Sweden), a tensile tester (L&W 004, Kista, Sweden), and a Z-span tester (PULMAC 2400, Hudson, Canada) in accordance with TAPPI T220 sp-96 (1996). The bonding capacities including the bonding strength index (B), the specific bonding strength per unit bonded area (b), and the relative bonded area (RBA) were calculated following Li *et al.*(2014). The equations for the calculation of B, b, and RBA are Eq. 2 and Eq. 3 (Li *et al.* 2014),

$$B = \left[\frac{1}{T} - \frac{9}{8Z}\right]^{-1} = \frac{bRBA}{k} = \frac{b}{k} - \left[\frac{b}{kS_0}\right]S \qquad (2)$$

$$RBA = \frac{S_0 - S}{S_0} \qquad (3)$$

where B is the bonding strength index of the handsheets (N·m/g), T is the tensile index of the handsheets (N·m/g), Z is the zero-span tensile index of handsheets (N·m/g), b is the specific bonding strength per unit bonded area (N/m^2), RBA is the relative bonded area (%), k is a parameter related to the fiber characteristics which is defined as $12c/(PL)$ (g/m^3), c is the fiber coarseness (μg/m), P is the fiber perimeter (μm), L is the fiber length (mm), S is the light-scattering coefficient of the handsheets (m^2/kg), and S_0 is the total light scattering coefficient for a completely unbonded fibers in a sheet (m^2/kg).

RESULTS AND DISCUSSION

The Inter-fiber Bonding Capacities of Poplar P-RC APMP Fiber Fractions

The tensile index (T), zero-span tensile index (Z), and the bonding capacities (B, b, and RBA) of four fiber fractions are listed in Table 1. The tensile index of four fiber fractions increased with a decrease in the fiber length, while the zero-span tensile index, which characterizes the strength of the fiber itself, demonstrated the opposite trend. Thus, for the fibers used in this study, the inter-fiber bonding capacities increased with decreased fiber length. The B, b, and *RBA* results confirmed this inference: the rate of increase for the three parameters from R30 to P100/R200 fiber fractions were 73%, 155%, and 40%, respectively.

Table 1. Inter-fiber Bonding Capacities of Poplar P-RC APMP Fiber Fractions

Fiber Fractions	R30	P30/R50	P50/R100	P100/R200
T (N·m/g)	7.75	10.24	11.47	12.07
Z (N·m/g)	118.6	109.1	95.3	82.4
B (N·m/g)	8.36	11.45	13.26	14.45
b (10^6N/m^2)	1.14	1.39	1.86	2.92
RBA (%)	15.28	18.72	19.35	21.21

Factors Influencing the Inter-fiber Bonding Capacities

The fiber morphology and the fiber charge of four fiber fractions were measured, and results are listed in Table 2. The fiber length and coarseness of four fiber fractions decreased from 1.067 mm to 0.396 mm and from 141.4 μg/m to 98.5 μg/m, respectively, with the increase of the sieve mesh number from 30 to 200, while the fiber width decreased obviously. However, the total and surface charges of four fiber fractions increased as the sieve mesh number increased. Generally, the fiber with a long fiber length and big width had a higher tensile strength because it had a high zero-span tensile strength; however, the tensile index of four fiber fractions shown in Table 1 increased as the fiber length and width was reduced. This result indicated that the size of the fiber (length and width) is not the most important factor for the inter-fiber bonding capacity. The parameters in Table 2, which showed the same trend as the tensile index and bonding strength index, are the key factors to the inter-fiber bonding capacity.

Table 2. The Influence Factors of the Inter-fiber Bonding Capacities

Fiber Fractions	R30	P30/R50	P50/R100	P100/R200
Length (mm)	1.067	0.873	0.675	0.396
Width (μm)	24.2	23.4	22.8	22.4
Coarseness (μg/m)	141.4	121.6	109.1	98.5
Total Charge (mmol/kg)	133±2	142±1	165±4	178±3
Surface Charge (mmol/kg)	31.8	37.5	43.9	48.6
Total Lignin (%)	21.09	22.46	23.58	24.27
Surface Lignin (%)	72.43	71.19	69.87	69.25
Standard Deviation of the Surface Lignin	0.335	0.399	0.410	0.369

Note: The sieve mesh numbers used in this study were 30, 50, 100, and 200.

The total lignin content and the surface lignin content or concentration of the four fiber fractions are also listed in Table 2. The results suggested that the surface lignin content determined by XPS was higher than the total lignin content of the pulp. Hence, some of the middle lamella and the primary wall of the fibers were preserved during the pulping process. The lignin concentration on the fiber surface of the long fiber fraction was slightly higher than that of the short fiber fraction, but this finding was not consistent for the total lignin. This result was due to the nature of the XPS measurement, which analyzes the lignin content on the surface of individual fibers (5 to 10 nm deep), while the measurement of total lignin measures the fiber fractions that have fiber debris generated during the pulping process. The surface lignin coverage decreased from 72.43% to 69.25% in correspondence with the fiber fraction from R30 to P100/R200. Lignin is enriched in the middle lamella, and the shorter fiber fractions produced by harsher pulping processes lost more middle lamella than the longer fiber fractions.

Figure 1 shows the distribution of the surface lignin of four fiber fractions analyzed by AFM. The surfaces of poplar P-RC APMP fibers were heterogeneous. Some flaky material was observed on the surface of all four fractions (marked by the red oval in Figure 1), especially in R30 and P30/R50. In addition to the flaky material, there were many granular objects on the fiber surface. Combined with the previous studies and the mechanism of AFM analysis, the flaky and granular materials on the fiber surfaces were identified as lignin and lignin-carbohydrate complexes (LCCs). Lignin is enriched in the middle lamella and the primary wall of the wood fibers. Thus, it was inferred that different cell wall layers are exposed along the fiber surface of poplar P-RC APMP.
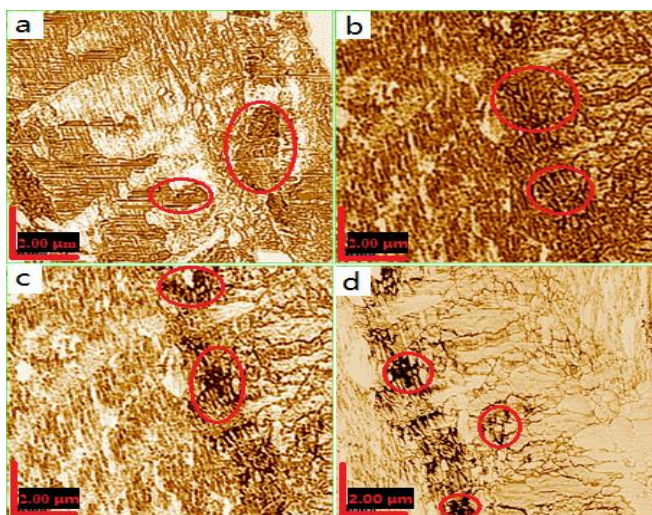
Fig. 1. Lignin distribution on the fiber surface of fractions (a) R30, (b) P30/R50, (c) P50/R100, and (d) P100/R200. The sizes of four AFM images are all 10x10 μm.

The surface of R30 fibers was almost fully covered by the flaky material, and there was little granular material. The amount and the area of the flaky material decreased as the fiber size decreased. For the P100/R200 fibers, there was hardly any flaky material, and the surface was coated with the granular material. These results suggested that more lignin was removed from the short fiber fractions than the long fiber fractions. These findings confirmed the results of the XPS analysis for the surface lignin content in Table 2.

Estimating the Effect of Surface Lignin on the Inter-fiber Bonding Capacities through PFI Beating

The P30/R50 fiber fraction was subjected to a peeling treatment (modified PFI beating) to investigate the influence of surface lignin on the inter-fiber bonding capacity. Figure 2 shows the relationship between the surface lignin concentration and the PFI beating revolutions.
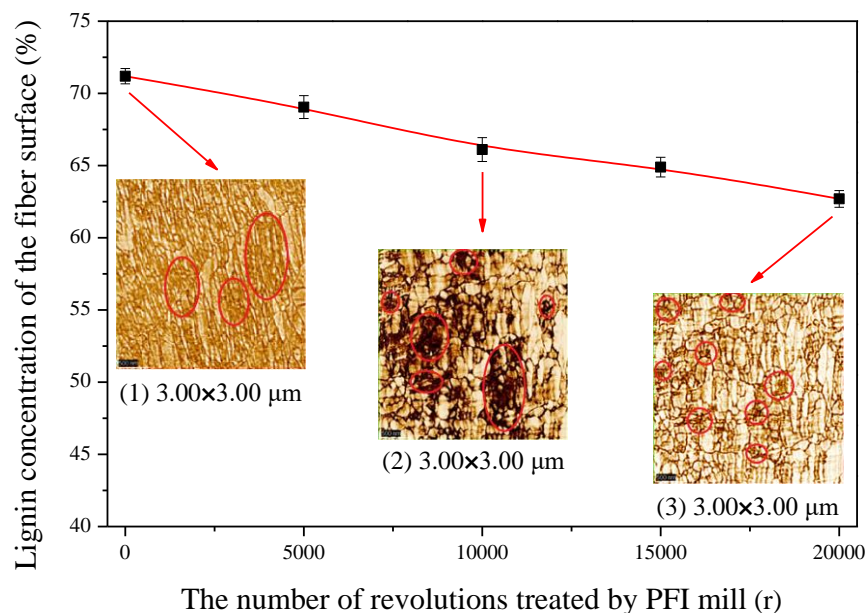
Fig. 2. Lignin concentration on the surface of fibers treated by PFI mill

In Fig. 2, the concentration of surface lignin decreased from 71.19% to 62.69%, corresponding with increasing PFI beating revolutions. The three AFM images shown in Fig. 2 are distributions of the lignin on the fiber surface of the P30/R50 fiber fraction that were untreated (0 revolutions), and treated with the modified PFI beating for 10,000 and 20,000 revolutions. The flaky material on the fiber surface disappeared with the enhanced peeling treatment. The material coating the surface became granular, and the distribution of the surface lignin appeared more uniform after the peeling treatment.

Table 3 presents the fiber morphology (including the length, width, coarseness, and the fines content), the fiber charge, and the lignin content of the P30/R50 fiber fraction that was treated by modified PFI beating to induce peeling. The fiber lengths shown in Table 3 are almost unchanged, while the fiber widths decreased slightly. Thus, the peeling treatment by the modified PFI beating had little influence on the fiber size. The slight decrease of the fiber width indicated that some material of the fibers was peeled away during the modified PFI beating. The fiber coarseness decreased substantially with the increase in the PFI beating revolutions, which confirmed the effect of the peeling treatment.

The peeling treatment changed some of the fiber properties, such as the total and surface lignin content, and the fiber charges. Both the total and surface lignin content decreased after the peeling treatment by PFI mill. Compared with the untreated sample, after 20000 revolutions PFI beating, the total and surface lignin content was reduced with the ratio of 25% and 12%, respectively. The total and surface charges of fibers increased to a different degree. With an increase in PFI beating revolutions, the total charge increased slightly, while the surface charge increased remarkably. The surface charge increase

resulted from surface lignin removal, which exposed cellulose and hemicellulose on the fiber surface. This data further demonstrated that the peeling treatment removes surface lignin. Furthermore, some carbohydrates (cellulose and hemicelluloses, in the form of microfibril) which were covered by the lignin and/or lignin-carbohydrate complexes (LCCs) before the removal of the surface lignin were released and shown on the new surface of the fibers.

Table 3. Factors Influencing the Inter-fiber Bonding Capacities after Treatment by PFI Mill

Revolutions (r)	0	5000	10000	15000	20000
Length (mm)	0.873	0.878	0.885	0.882	0.875
Width (μm)	23.4	23.3	23.2	23.1	22.9
Coarseness (μg/m)	121.6	114.6	111.5	109.0	99.1
Total Charge (mmol/kg)	142±1	144±2	146±3	147±2	150±2
Surface Charge (mmol/kg)	37.5	47.8	51.2	56.6	62.3
Total Lignin (%)	22.46	21.29	19.72	18.49	16.84
Surface Lignin (%)	71.19	69.05	66.11	64.89	62.69
Standard Deviation of the Surface Lignin	0.399	0.306	0.384	0.421	0.282

Table 4. Inter-fiber Bonding Capacities of P30/R50Fraction Treated by PFI Mill

Revolutions (r)	0	5000	10000	15000	20000
T (N·m/g)	10.24	16.27	18.57	22.05	23.02
Z (N·m/g)	109.1	105.1	93.1	88.1	82.8
B (N·m/g)	11.45	19.69	23.97	31.56	32.65
b (106 N/m^2)	1.39	2.39	2.71	2.88	2.89
RBA (%)	18.72	19.95	21.42	23.85	26.19

The peeling treatment of the P30/R50 fiber fraction improved the strength and inter-fiber bonding properties. Table 4 lists the tensile index (T), the zero-span tensile index (Z), and the bonding capacities (B, b, and RBA) of the P30/R50 fiber fraction with different degrees of peeling treatment. The tensile index (T) of the P30/R50 fiber fraction increased with the enhancement of the peeling treatment through the modified PFI beating, while the zero-span tensile index (Z) diminished. This result indicated that for the poplar P-RC APMP fibers used in this study, inter-fiber bonding capacities were improved with modified PFI beating. The B, b, and RBA data proved that the peeling treatment resulted in high inter-fiber bonding capacities, and the amplitude of the improvement depended on the intensity of the peeling treatment. The B, b, and RBA increased by 110%, 95%, and 15%, respectively, after 10,000 revolutions (r) modified PFI beating, while the enhanced ratio was 185%, 110%, and 40%, respectively, when the revolution changed to 20,000. Furthermore, b increased when the PFI beating revolution was lower than 10,000. When r was greater than 10,000, the enhanced ratio did not increase as much, and the b came to a stable value. Combining the data in Table 3 and Table 4, it can be inferred that the surface lignin content and the surface charge of fibers are the two key factors affecting inter-fiber bonding capacities.

bioresources.com

CONCLUSIONS

1. Four high-yield pulps fiber fractions had different characteristics and inter-fiber bonding capacities. The surface lignin content of the long fiber fraction was slightly lower than that of the short fiber fraction. AFM images showed that the surface of poplar P-RC APMP fibers were heterogeneous; different cell wall layers were exposed along the fiber surface. The number and the area of the flaky material found on the fiber surface decreased with decreasing fiber size. The fiber fraction with the lower surface lignin content had higher bonding capacities.

2. After the modified PFI peeling treatment, the surface charge of the fibers increased from 37.5 mmol/kg to 62.3 mmol/kg, while the lignin concentration on the fiber surface decreased substantially. The surface lignin concentration and the surface charge of lignocellulosic fibers are the two key factors for estimating the inter-fiber bonding capacities.

ACKNOWLEDGMENTS

REFERENCES CITED

Faruk, O., Bledzki, A. K., Fink, H. P., and Sain, M. (2014). "Progress report on natural fiber reinforced composites," *Macromolecular Materials and Engineering* 299(1), 9-26. DOI: 10.1002/mame.201300008

GB/T 747-1989 (1989). "Pulps-Determination of acid-insoluble lignin," Standards Press of China, Qinhuangdao, China.

GB/T 10337-1989 (1989). "Raw material and pulp-Determination of acid-soluble lignin," Standards Press of China, Qinhuangdao, China.

GB/T 10741-1989 (1989). "Pulps – Determination of alcohol-benzenes solubles," Standards Press of China, Qinhuangdao, China.

Hubbe, M. A. (2007). "Bonding between cellulosic fibers in the absence and presence of dry-strength agents –A review," *BioResources* 1(2), 281-318. DOI: 10.15376/biores.1.2.281-318

Lei, Y., Qian, X., Shen, J., and An, X. (2012). "Integrated reductive/adsorptive detoxification of Cr(VI)-contaminated water by polypyrrole/cellulose fiber composite," *Industrial &Engineering Chemistry Research* 51(31), 10408-10415. DOI: 10.1021/ie301136g

Li, H., Zhang, H., Li, J., and Du, F. (2014). "Comparison of interfiber bonding ability of different poplar P-RC alkaline peroxide mechanical pulp (APMP) fiber fractions," *BioResources* 9(4), 6019-6027. DOI: 10.15376/biores.9.4.6019-6027

Li, J., Zhang, H., Li, J., Hu, H., and Cao, Z. (2015). "Fiber characteristics and bonding strength of poplar refiner-chemical preconditioned alkaline peroxide mechanical pulp fractions," *BioResources* 10(2), 3702-3712. DOI: 10.15376/biores.10.2.3702-3712

Li, Z., Zhang, H., Wang, X., Zhang, F., and Li, X. (2016). "Further understanding the response mechanism of lignin content to bonding properties of lignocellulosic fibers by their deformation behavior," *RSC Advances* 6(110), 109211-109217. DOI: 10.1039/C6RA22457A

Qazi, T. H., Mooney, D. J., Pumberger, M., Geissler, S., and Duda, G. N. (2015). "Biomaterials based strategies for skeletal muscle tissue engineering: existing technologies and future trends," *Biomaterials* 53, 502-521. DOI: 10.1016/j.biomaterials.2015.02.110

Ragauskas, A. J.,Williams, C. K., Davison, B. H., Britovsek, G., Cairney, J., Eckert, C. A., Frederick Jr., W. J., Hallett, J. P., Leak, D. J., Liotta, C. L., *et al.* (2006). "The path forward for biofuels and biomaterials," *Science* 311(5760), 484-489. DOI: 10.1126/science.1114736

Ranganathan, N., Oksman, K., Nayak, S. K., and Sain, M. (2016). "Structure property relation of hybrid biocomposites based on jute, viscose and polypropylene: The effect of the fibre content and the length on the fracture toughness and the fatigue properties," *Composites Part A: Applied Science and Manufacturing* 83, 169-175.

Shao, Z., and Li, K. (2006). "The effect of fiber surface lignin on interfiber bonding," *Journal of Wood Chemistry and Technology* 26, 231-244.

Shen, J., and Fatehi, P. (2013). "A review on the use of lignocellulose-derived chemicals in wet-end application of papermaking," *Current Organic Chemistry* 17(15), 1647-1654. DOI: 10.2174/13852728113179990075

Shen, J., Fatehi, P., and Ni, Y. (2014). "Biopolymers for surface engineering of paper-based products," *Cellulose* 21(5), 3145-3160. DOI: 10.1007/s10570-014-0380-6

TAPPI 205 sp-95 (1995). "Forming handsheets for physical tests of pulp," TAPPI Press, Atlanta, GA.

TAPPI 220 sp-96 (1996). "Physical testing of pulp handsheets," TAPPI Press, Atlanta, GA.

TAPPI 233 om-95 (1995). "Fiber length of pulp by classification," TAPPI Press, Atlanta, GA.

Zhao, C., Zhang, H., Zeng, X., Li, H., and Sun, D. (2016). "Enhancing the inter-fiber bonding properties of cellulosic fibers by increasing different fiber charges," *Cellulose* 23(3), 1617-1628. DOI: 10.1007/s10570-016-0941-y